IEEE Access
Multidisciplinary ⋮ Rapid Review ⋮ Open Access Journal

Received 29 January 2025, accepted 22 February 2025, date of publication 27 February 2025, date of current version 7 March 2025.

Digital Object Identifier 10.1109/ACCESS.2025.3546456

RESEARCH ARTICLE

Estimating Remaining Usable Time of Batteries With Uncertainty Quantification: A Case Study on Base Transceiver Station Application Using Real-Life Data

YONAS TEFERA[1,2], (Member, IEEE), STIJN LUCA[3], DEREJE HAILEMARIAM WOLDEGEBREAL[2], AND PETER KARSMAKERS[1,4,5]

[1]Department of Computer Science, KU Leuven, 2440 Geel, Belgium
[2]School of Electrical and Computer Engineering, Addis Ababa University, Addis Ababa 1000, Ethiopia
[3]Department of Data Analysis and Mathematical Modelling, Ghent University, 9000 Gent, Belgium
[4]Leuven.AI, 2440 Geel, Belgium
[5]Flanders Make@KU Leuven, 2440 Geel, Belgium

Corresponding author: Yonas Tefera (yonas.tefera@kuleuven.be)

ABSTRACT Systems consisting of multiple components can experience downtime during their operational lifetime due to issues with one or more of these components. For instance, accurately predicting the remaining time before a battery depletes its total energy is crucial for systems like a Base Transceiver Station. This paper addresses how long the battery will sustain a Base Transceiver Station under varying load conditions with the associated uncertainty when the external power source is interrupted. A customized approach using battery modeling and load forecasting is designed to predict the remaining usable time of the battery. In total, 7 Base Transceiver Stations are considered and clustered into 3 groups based on their installed battery capacity. First, a battery model is developed employing the modified Shepard model using real-life measured battery discharge data. Since the load currents are unknown beforehand, they are forecasted using a time series modeling approach. The resulting uncertainty from both models is then quantified using a prediction interval. Using our approach, the averaged Mean Absolute Error of the remaining usable time estimates is 12.61 minutes for all discharges. The associated uncertainty with these estimation using the 95% prediction interval is 26.43 minutes. The estimation errors are relatively small compared to true discharge times, as some batteries can provide energy close to 15 hours. The overall estimation results closely matched the measured values, providing valuable insights for proactive planning and management of potential failures.

INDEX TERMS Base transceiver station, battery models, load forecasting, remaining usable time, uncertainty quantification, predictive maintenance.

I. INTRODUCTION

As a telecom network infrastructure expands, the task of monitoring and maintaining becomes increasingly challenging due to the growing number of fault indicating alarms generated every day. Diagnosing and clearing those alarms from different subsystems of the network by corrective maintenance activities require considerable effort and resources. A Base Transceiver Station (BTS) is a crucial infrastructural unit in mobile networks that facilitates wireless communication between user equipment and the mobile network. The BTS system constitutes a number of different components which should be continuously monitored and proper corrective action should be taken in case a fault occurs. Without proactive actions, the service to customers can be interrupted.

The associate editor coordinating the review of this manuscript and approving it for publication was Gaetano Zizzo.

The disconnect of the power system as a result of frequent external power blackouts accounts for the largest share of BTS service interruptions for a telecom service provider in Addis Ababa, Ethiopia. Thus, anticipating and predicting upcoming service interruptions due to power system issues and taking corrective actions will help ensure the quality of service, leading to increased revenue. An interruption in BTS service due to the power system occurs as a result of a series of interconnected issues. An external power disconnect or failure of the main power unit component will activate the secondary power source (a generator) of the site. During the transition to the secondary power source or in the event of its complete failure to provide power, the BTS load is transferred to a battery bank. When the power monitoring system generates an alarm about an external power interruption and a secondary power source malfunction, an engineer is responsible for estimating the time frame during which the site can remain operational before the service is completely interrupted. Based on this estimate, a decision can be made to wait for external power to return (depending on the utility company's response) or, if possible, perform maintenance to fix the secondary power system before the battery bank is depleted. This decision is not automated and depends on detailed knowledge of the site and the experience of the engineer. Even an experienced engineer can only have a rough estimate of how long the battery will sustain the site load before a service interruption occurs. This is because complete information on the battery's present effective capacity, state-of-charge (SoC), and expected BTS load characteristics are not readily available. In the event of a power outage at multiple BTS sites, it is even more critical to have detailed information on the different site availability windows to prioritize interventions.

In this work, an automated estimate of the remaining usable time (RUT) is addressed before the depletion of the energy of the BTS batteries. The proposed method predicts the battery bank voltage progression under varying forecasted load currents until it reaches a voltage level that corresponds to an energy level that causes service interruption. The time until this point is the estimated RUT. To obtain the RUT estimate, the uncertainties related to the load forecast and voltage progression prediction are taken into account, as shown in Figure 1. The RUT estimation is initiated at $t = t_0$ using the battery capacity depletion data until that point and a mathematical model. At $t = t_e$, the battery reaches a cut-off voltage. The RUT is defined as $t_e - t_0$ and is stochastic in nature. To characterize the uncertainty of the estimated RUT, a Probability Density Function (PDF) of the RUT is determined. Instead of providing a single value, it is desirable to present a RUT prediction interval [1] within the bounds of the lower (t_{le}) and upper (t_{ue}) quantile ranges.

The literature in this area mainly focuses on predicting the remaining useful life of a battery [2], [3], [4]. However, reliably monitoring and accurately forecasting the battery capacity over a short time horizon is also crucial in battery-powered systems. Several existing techniques for predicting

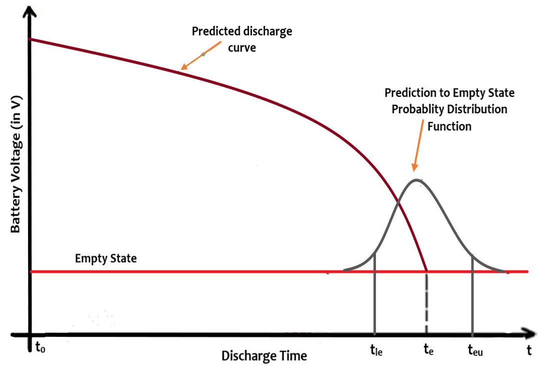

FIGURE 1. Typical predicted battery voltage discharge curves with 95% prediction interval.

the remaining capacity of lead-acid and lithium-ion batteries discharged with a variable current are based on variants of Peukert's empirical equation [5]. In [6] the authors present exponential decay equations that model the behavior of the battery capacity drop with the discharge current and show that these equations have a superior accuracy compared to the empirical Peukert equation. A closed-form analytical expression for predicting the remaining capacity of a lithium-ion battery is presented by [7]. Chemical kinetics [8], [9] based models are also usable for short-term capacity prediction. Approaches such as [10], [11], and [12] use an equivalent circuit model and state-space equations to build a Kalman filter to fuse model predictions and measurements for enhanced capacity estimation. When there is a large pool of battery data available, deep learning-based approaches can be applied such as in [13], [14], [15], and [16]. In the context of telecommunication power systems, there are studies that estimate the SoC of a battery [17], [18]. Furthermore, other works use SoC estimates to determine RUT under constant load current discharges in controlled environments [19]. In this work, we developed a novel method not addressed in the existing literature to automatically estimate the RUT of a lead-acid battery in real-world situations where the load currents vary over time and are unknown for future time steps. Furthermore, the uncertainty of the RUT estimation is quantified by providing a prediction interval and the method is empirically evaluated using real-life data.

The remainder of the paper is organized as follows. In Section II, we present the proposed methodology that involves a battery modeling algorithm and a load forecasting model to estimate the RUT. Section III discusses the examined use-case scenario, focusing on the BTS power unit, the collected data, and its properties. Section IV presents and discusses the implementation of the proposed methodology and the results obtained from the RUT estimation approach. Finally, in Section V, we formulate a conclusion by summarizing the results from the conducted set of experiments.

II. METHODOLOGY

In this work, we propose an approach to estimate the RUT and quantify the uncertainty of this estimate by computing a prediction interval. To accomplish this task, two main components are required: a) a battery model that can keep track of the SoC of a battery and the voltage progression, and b) a load forecasting model that predicts future (unknown) loads. In both parts, uncertainties are present, and both will be quantified.

A. BATTERY MODEL

The battery modeling literature discusses various approaches for modeling SoC and voltage progression in batteries, including physics-based, data-driven, and hybrid methods [20], [21], [22]. This work adopts a physics-based modeling approach that requires fewer data compared to a data-driven approach. Within this category, electrochemical and equivalent circuit models are the most prevalent where a more detailed exploration and review is given in [23], [24], and [25]. The proposed approach uses a battery model based on the Shepherd equation, but is flexible and can also use other models. Shepherd developed a mathematical equation to describe the electrochemical behavior of a battery directly in terms of terminal voltage, open circuit voltage, internal resistance, discharge current, and SoC [26]. A modified version of this equation, known as the modified Shepherd equation [27], is used to determine the battery discharge voltage, and is expressed as follows:

$$\hat{v}_{\text{batt}}(t) = V_0 - K \cdot \frac{Q_B}{Q_B - \int_0^t i_{\text{batt}}(t)\, dt} i_{\text{batt}}(t) - R_i i_{\text{batt}}(t) + A e^{-B \int_0^t i_{\text{batt}}(t)\, dt}, \tag{1}$$

where $\hat{v}_{\text{batt}}$ is the (predicted) battery voltage (in volts), i_{batt} is the battery current (in amperes), V_0 is the open circuit voltage at full capacity (in volts), K is the polarization constant (in volts per ampere-hour), Q_B is the maximum battery capacity (in ampere-hour), $\int_o^t i_{\text{batt}}\, dt$ is the discharged battery capacity (in ampere-hour), A is the exponential zone amplitude (in volts), B is the exponential capacity (in inverse ampere-hours), and R_i is the internal resistance (in ohms).

In Figure 2, a prototypical battery discharge curve is presented. It contains three main sections: an initial exponential region, a nominal region, and a final exponential region, typical features observed in the discharge profiles of this work. Each of these sections are represented by the last three terms in Equation (1).

The SoC estimation uses the Coulomb counting method [28] at time t and is expressed as:

$$\text{SoC}(t) = \text{SoC}_{\text{init}} - \frac{1}{Q_B} \int_0^t i_{\text{batt}}(t)\, dt. \tag{2}$$

where SoC_{init} is the initial SoC.

After selecting the battery modeling approach, the model parameters need to be determined. If the required parameters cannot be obtained from the manufacturer's datasheet, a data-driven approach is necessary to determine the parameter values by using the collected battery-related data. The model parameters V_0, Q_B, and R_i are assumed to be deterministic.

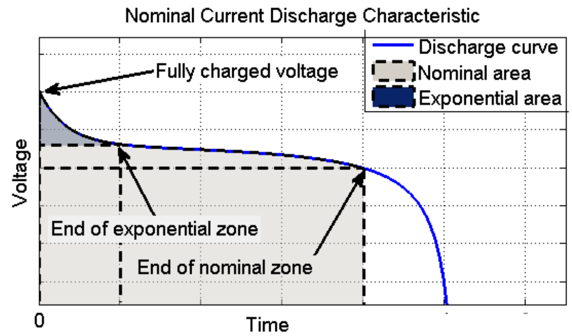

FIGURE 2. A typical pattern of a discharge curve [27].

V_0 is the open-circuit voltage and is obtained from the battery voltage measured at full capacity. Q_B is obtained by summing up the total charge exhausted when the battery goes through a full discharge and R_i is also calculated using:

$$R_i = \frac{1}{n} \cdot \sum_{j=1}^{n} \frac{v_{\text{batt}}(j) - v_{\text{batt}}(j-1)}{i_{\text{batt}}(j)} \tag{3}$$

where n is the number of data sample points in a discharge curve, $v_{\text{batt}}(j)$ and $i_{\text{batt}}(j)$ are the observed voltage and current values at sample step j.

To determine the remaining parameters K, A, and B, a least-squares optimization procedure is used; such that the mean squared error between the model's estimated output voltages and those measured during real battery discharges is minimized:

$$\theta^* = \arg\min_{\theta} \sum_{j=1}^{n} (v_{\text{batt}}(j) - \hat{v}_{\text{batt}}(i_{\text{batt}}(j); \theta))^2 \tag{4}$$

where θ represents the set of parameters (K, A, and B) of the model that need to be optimized, θ^* are the optimized parameter values, and $\hat{v}_{\text{batt}}(i_{\text{batt}}(j); \theta)$ is the predicted battery voltage when the battery parameters θ are known.

In the context of battery modeling, there are several alternative approaches available to the modified Shepherd mathematical model. With recent advances in computational power and access to large datasets, data-driven deep learning architectures have become increasingly popular. These methods have significantly enhanced the performance of battery modeling [29]. However, in our specific case, the number of discharge events is relatively small. As a consequence, the complexity of the deep learning model must be kept relatively low. In the experimental section, a conventional feedforward neural network (FNN) [30] was evaluated for predicting battery voltage. This prediction is based on the estimated SoC, which is calculated using the Coulomb counting method. The feedforward network serves as a baseline model, enabling a performance comparison with the modified Shepherd model. This comparison provides valuable insights into the strengths and limitations of the latter approach.

To quantify the uncertainty in estimated battery voltages, a bootstrapping approach [31] is used. Instead of estimating the parameters of the battery model once, the parameters θ are estimated multiple times using subsamples of available data. In this way, each parameter can be described by a distribution of parameter values. During model inference, parameter values can be sampled from the parameter distributions to obtain a distribution of model outputs (battery voltages) that quantifies the uncertainty of the model output. Since a discharge curve comprises three main sections, as shown in Figure 2, stratified sampling is a suitable method to obtain model parameters from discharge curves. This approach ensures a balanced representation of each section within the sample sets, producing sample discharges that closely match the observed ones, and thus improving the accuracy of parameter estimation.

B. LOAD FORECASTING MODEL

To estimate the RUT using the battery discharge curve under varying load conditions, it is essential to develop a load forecasting model based on historical measurements. When external power is disconnected, the battery takes over and supplies the load. As a result, forecasting the load current is equivalent to forecasting the battery current (i_{batt}). This task involves time-series forecasting, a technique used for decision making based on forecasted values.

Depending on the task required, forecasting techniques can have different timescales: very short (up to an hour), short (up to six hours) and longer (one or more days) forecasts. Regression and/or multiple regression models are still widely used and efficient for long- and very-long-term forecasts [32]. Autoregressive (AR) models, artificial neural networks (ANNs) and support vector machines (SVMs) are the preferred models for making short-term and very short-term forecasts. AR models require to properly select the lagged inputs to identify the correct model orders, a procedure that demands a certain level of skill and expertise. Moreover, they make explicit assumptions about the nature of the system under examination. On the other hand, ANNs and their variants have been used in many contexts where the temporal dependency in the data is an important implicit feature in the model design. Contrarily to other linear models adopted for prediction, ANNs can learn functions of arbitrary complexity, and they can deal with time series properties such as exponential effects and nonlinear interactions between latent variables. However, if the temporal dependencies of the data are prevalently contained in a finite and short time interval, the use of ANNs can become unnecessary [33]. In addition, compared to AR models, ANN models require a larger data set for training.

In this work, a daily cyclic load pattern is observed that is determined by a large pool of users (e.g., of a mobile network). Due to the relatively limited amount of available real-life data and the expected short-time discharge load forecasts, a SARIMAX (Seasonal Autoregressive Integrated Moving Average with Exogenous Regressors) model is used [34]. The SARIMAX model is generally denoted as $(p, d, q)(P, D, Q, s)$, where p, d, q and P, D, Q are nonnegative integers that refer to the polynomial order of the autoregressive (AR), integrated (I) and moving average (MA) parts of the non-seasonal and seasonal components of the model, respectively, and s is the length of the seasonal cycle. It is mathematically formulated as [35]:

$$y_t = c + \sum_{i=1}^{p} \phi_i y_{t-i} + \sum_{j=1}^{q} \theta_j \epsilon_{t-j} + \sum_{k=1}^{P} \Phi_k y_{t-k\cdot s} + \sum_{l=1}^{Q} \Theta_l \epsilon_{t-l\cdot s} + \sum_{m=1}^{K} \beta_m X_m + \epsilon_t \tag{5}$$

where:
- y_t: is the forecast value at time t.
- c: constant term (intercept).
- ϕ_i: coefficients for autoregressive terms.
- θ_j: coefficients for moving average terms.
- ϵ_{t-j}: lagged noise terms.
- Φ_k: coefficients for seasonal autoregressive terms.
- Θ_l: coefficients for the seasonal moving average terms.
- $\epsilon_{t-l\cdot s}$: noise terms lagged by multiples of the seasonality period s.
- β_m: coefficients for exogenous variables.
- X_m: exogenous variables.
- ϵ_t: noise (white noise).

When applying AR-based models in forecasting, uncertainty arises from the estimation of the model parameters. Furthermore, when making forecasts in future time horizon, additional uncertainty arises from the inherent randomness in future observations. Thus, in this work, these uncertainties are quantified by a prediction interval.

C. RUT ESTIMATION

To estimate the RUT and its associated uncertainty, quantified by a prediction interval, it is necessary to properly combine the battery voltage and the forecast load currents. A prediction interval provides an estimated range within which future observations are expected to fall with a specified probability, given the existing data and model assumptions. Thus, they will provide a quantifiable measure of the uncertainty associated with individual RUT estimates. This approach is summarized in Algorithm 1 and illustrated in Figure 3.

The threshold voltage specified as T in Figure 3, represents the minimum voltage level at which the battery can no longer sustain the load, leading to the disconnection of the load at that point. From the simulated data in $\mathcal{H}$ (see Algorithm 1), the mean RUT (RUT_{mean}), as well as a prediction interval, can be estimated. The endpoints of the prediction interval can be computed by using appropriate quantiles [1]:

$$\text{Prediction Interval} = [Q_{\alpha/2}, Q_{1-\alpha/2}], \tag{6}$$

where $Q_{\alpha/2}$ and $Q_{1-\alpha/2}$ are the $\alpha/2$ and $1-\alpha/2$ quantiles of the distribution, respectively. They determine the lower and

Algorithm 1 RUT Estimation With Prediction Interval

$\mathcal{H} \leftarrow \emptyset$.
Estimate future load currents using Equation (5) at time steps $h = 0, \ldots, l-1$.
$K \leftarrow k$ // k being the sample size of the load currents.
while $K \neq 0$ **do**
  Draw a sample from all l current distributions to have $\forall h$, $\hat{i}_{\text{batt}}(t+h)$.
  $Z \leftarrow z$ // z being the sample size for the parameters of the battery model.
  while $Z \neq 0$ **do**
    Draw a sample for each battery model parameter from the battery model parameter distributions obtained by Equation (4).
    Calculate $\forall h$, $\hat{v}_{\text{batt}}(t+h)$ using Equation (1).
    Find smallest future time step h' where $\hat{v}_{\text{batt}}(t+h')) < T$.
    $\mathcal{H} \leftarrow h' \cup \mathcal{H}$.
    $Z \leftarrow Z - 1$.
  end while
  $K \leftarrow K - 1$.
end while
$n \leftarrow kz$.
Using $\mathcal{H}$ calculate $\text{RUT}_{\text{mean}} \pm$ Prediction Interval, RUT_{ME} and RUT_{MPE}

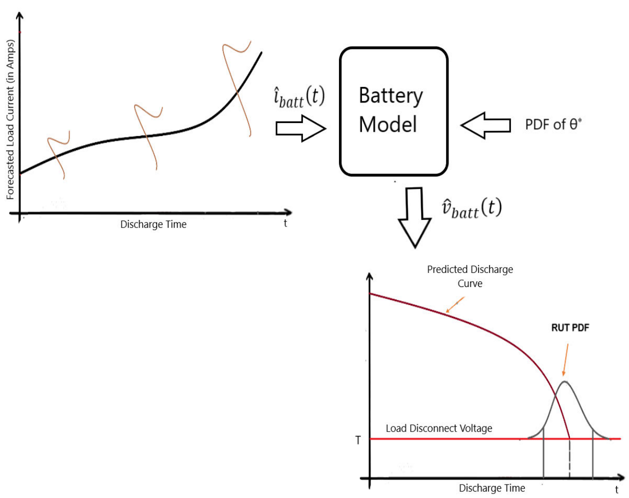

FIGURE 3. The devised RUT estimation approach.

upper bounds of the interval, respectively. These quantiles correspond to the critical values that enclose the middle $1-\alpha$ portion of the distribution. A value of $\alpha = 0.05$ is used to construct a 95% prediction interval. The lower bound of the interval corresponds to the $\alpha/2 = 0.025(2.5\%)$ quantile of the distribution, and the upper bound corresponds to the $1-\alpha/2 = 0.975(97.5\%)$ quantile.

Furthermore, two additional metrics are also used to evaluate model performance: the mean error (ME) defined in Equation (7) and the mean percentage error (MPE) defined in Equation (8).

$$\text{ME} = \frac{1}{n}\sum_{j=1}^{n}\left(\text{pRUT}_j - \text{tRUT}\right) \tag{7}$$

$$\text{MPE} = \frac{1}{n}\sum_{j=1}^{n}\left(\frac{\text{pRUT}_j - \text{tRUT}}{\text{tRUT}}\right) \times 100 \tag{8}$$

where tRUT is the true RUT and pRUT_j is the predicted RUT for sample discharge j.

ME measures the magnitude of RUT errors in the set of estimations. A positive ME value indicates an overestimation by the model, while a negative value indicates an underestimation. MPE measures the average percentage error between the predicted and actual values. It is scale-independent and provides insight into the accuracy of the estimation in percentage terms.

III. USE-CASE: RUT ESTIMATION IN BTS

A. BTS POWER SYSTEM

A BTS system is composed of various components including cellular network equipment, transmission equipment (used as a backbone or link to other BTSs), and power supply unit equipment. The power supply unit is responsible for providing the electrical power required to the different subsystems. This work focuses primarily on service interruptions caused by issues within the power supply unit.

The schematic architecture of the power supply unit is shown in Figure 4. Energy is sourced from the AC distribution unit, which distributes AC power from the commercial power system, the generator, renewable energy sources, or any combination of these three to the rectifiers. The AC distribution unit includes automatic transfer switches, a surge arrestor power protection unit, and an AC bus-bar. The current measured on the AC bus-bar is denoted as $i_{AC}(t)$. Using the rectifier banks, AC is converted to DC in the DC distribution unit. The latter unit distributes DC power from the rectifiers or battery bank to different attached DC loads. The voltage and current measured on the DC bus-bar are $v_{DC}(t)$ and $i_{DC}(t)$, respectively. The voltage and current measured in the battery bank are $v_{\text{batt}}(t)$ and $i_{\text{batt}}(t)$, respectively. The type of battery used in the BTS power systems is a lead-acid battery. A real-time monitoring unit monitors the operational status and environmental condition (such as the battery temperature $T_{\text{batt}}(t)$, the total discharge of the battery $Q_{d,\text{tot}}(t)$, and the total battery cycle times $N_{\text{cycles}}(t)$ of the system using different sensors and measurement tools.

A number of different faults can arise in the power system unit of a BTS, which can cause service interruption. In the event of a power outage from both the primary and secondary sources, the BTS battery serves as the final backup to prevent load disconnect and service interruption. A disconnect occurs when the battery voltage drops below a pre-defined threshold. This scenario is deemed critical and has the potential to result in a partial or complete interruption of service if no timely intervention measures are implemented.

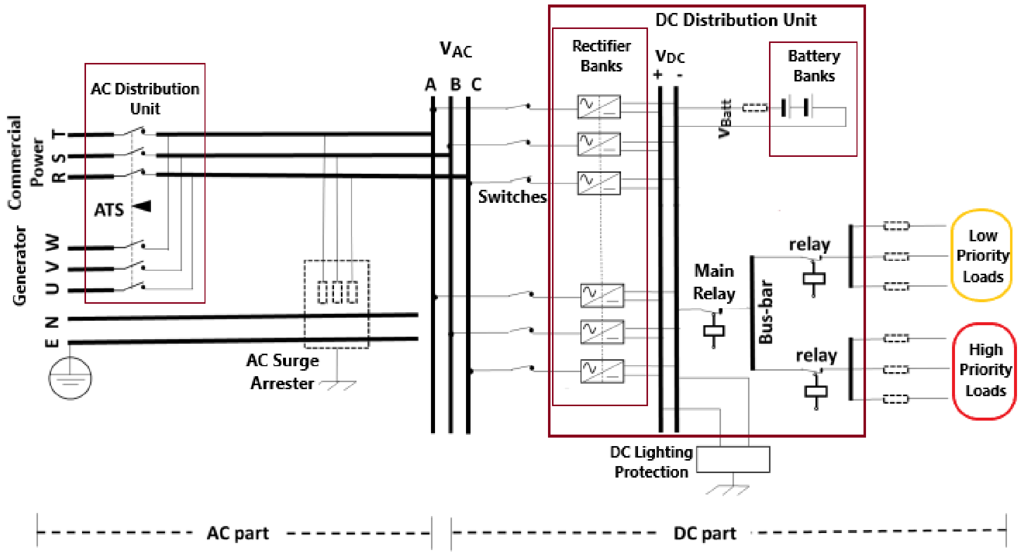

FIGURE 4. BTS power system architecture [36].

B. BTS DATA

The dataset used in this work is obtained from the BTS power unit monitoring system [36]. Time series data is collected for 7 BTS sites for 16 weeks (from April to July 2019). The data set contains 8 signals ($i_{AC}(t)$, $v_{DC}(t)$, $i_{DC}(t)$, $v_{\text{batt}}(t)$, $i_{\text{batt}}(t)$, $T_{\text{batt}}(t)$, $Q_{d,\text{tot}}(t)$ and $N_{\text{cycles}}(t)$) with a five-minute sampling period. In Figure 5, an example dataset for a single BTS is provided, showing the 8 signals during the collection period.

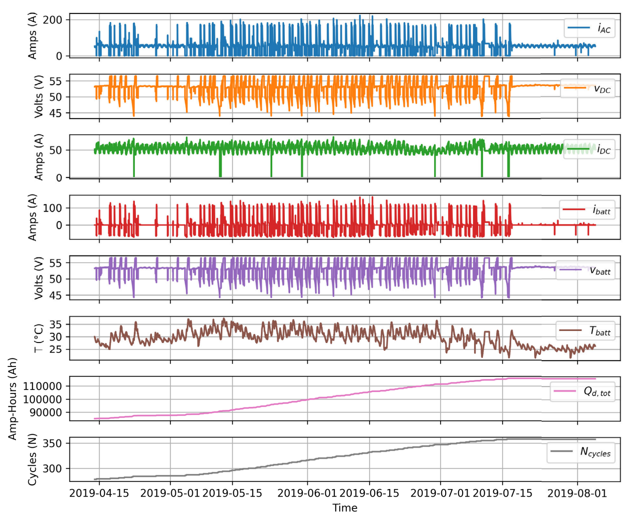

FIGURE 5. BTS power system data.

To streamline the analysis and minimize the number of battery models required, BTS units are organized into clusters. The clusters are formed based on the total installed capacity of the battery bank in each BTS. As a result, three distinct clusters are created, with each BTS assigned to one of these groups. The estimated battery capacity is determined by measuring the battery discharges starting from a fully charged state until they reach a voltage level that causes the load to disconnect. The characteristics of the 3 clusters are summarized in Table 1. In addition to the number of BTSs in the clusters, we also list the capacity of the battery bank and the number of discharges recorded within the observation window that led to service interruption.

TABLE 1. Characteristics of created BTS clusters.

Cluster ID	No. of BTSs	Battery Capacity (in Ah)	Total No. of discharges causing service interruption
C1	1	300	7
C2	3	750	4
C3	3	720	10

In one BTS within cluster C3, frequent interruptions were observed. Although these interruptions did not often lead to service outages, they did accelerate the aging process of the battery, resulting in a gradual reduction in its capacity over time. As the battery cycle time increases, its capacity decreases. This trend is observed in Figure 6, which shows the variation in discharge capacities over time. In a cluster, discharge profiles with similar capacities, inferred from the cycle times, are assumed to come from batteries of the same age and are used in battery modeling phase. Although there are existing battery models that account for the effects of aging, this study does not include aging as a factor. Consequently, discharges associated with aged batteries have been excluded from this analysis.

Furthermore, when analyzing the data, it was observed that at lower battery SoCs, the initial discharge voltages were unexpectedly close to fully charged levels, despite lower voltages being anticipated. This is shown in Figure 7, which plots the battery voltage against the normalized SoC.

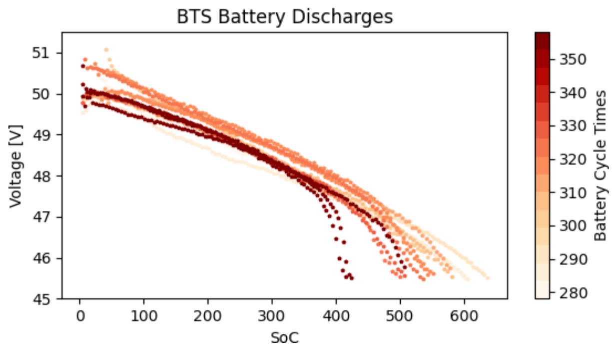

FIGURE 6. Capacity degradation or aging of a single BTS battery bank.

Discharges are plotted until the first load disconnect voltage point of $46.2V$. The normalized SoC at time t is calculated by dividing SoC(t) by the maximum SoC of the battery (Q_B). This voltage-to-SoC discrepancy is attributed to the smoothing effect of the rectifier, which prevents a sharp voltage drop. As the battery approaches full discharge, this effect diminishes and the bus-bar voltage mirrors the battery's terminal voltage. Since RUT estimation is based on voltage values near full discharge, the proposed battery modeling approach remains valid.

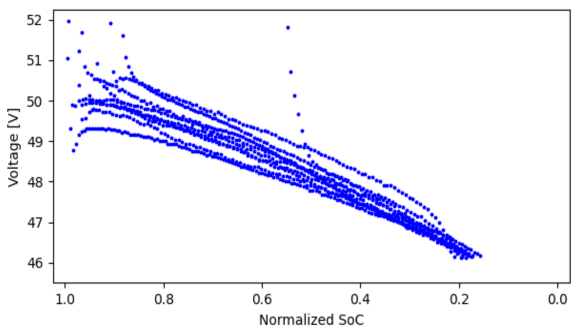

FIGURE 7. BTS battery discharge voltages starting from different SoC values.

IV. EXPERIMENTS AND RESULTS

This section starts by describing the process used to obtain the parameters of the battery model using the available real-life data. Then, the load forecasting model is developed along with its associated parameters. Finally, the outcomes of both models are combined to estimate the RUT. For clarity, only intermediate results of the plots for cluster C1 are presented. The final RUT estimates with associated prediction intervals and model performance metrics are provided for all three clusters.

A. BATTERY MODEL PARAMETER IDENTIFICATION

The battery model used in Equation (1) has the following parameters that need to be identified: V_0, K, Q_B, A, B, and R_i. For the use case scenario considered in this work, it was not possible to identify parameters through controlled experiments, and detailed specifications for the batteries were also lacking. To identify the parameters (K, A, and B) for each cluster, a Leave-One-Out Cross-Validation approach [37] is applied to the discharge data records collected during the operation of the BTS. This method is especially suitable given the small number of discharges per cluster. For a cluster with n discharges, the model is trained on $n-1$ discharges, leaving one discharge out as the test set. This process is repeated n times, and each discharge is used as a test set once. The parameter values are determined using the least squares optimization approach introduced in subsection II-A. The parameter V_0 is obtained from the voltage measurement when the battery is fully charged. The internal resistance R_i is calculated using Equation (3) and is assumed to be constant. Therefore, it does not vary with the changing load current. The values of these deterministic parameters are given in Table 2.

TABLE 2. V_0, Q_B and R_i values of the BTSs in each clusters.

Cluster ID	V_0 (in V)	Q_B (in Ah)	R_i (in $m\Omega$)
C1	50	300	1.503
C2	51.5	750	0.742
C3	51	720	0.794

The SoC of a battery is an important parameter for accurately predicting the voltage progression. From the available battery data, Equation (2) is used as the SoC estimation approach in this work. The accuracy of this method relies primarily on a precise measurement of the battery current and an accurate estimation of the initial SoC. The battery currents are part of the BTS data, but the initial SoC values are not provided. When the battery is neither charging nor discharging and the external power is ON, it is assumed to be fully charged. This point serves as a reference to calculate the progression of the SoC during charging and discharging using the coulomb counting method. However, this approach may not always yield an accurate initial estimate, potentially due to the long sampling time of 5 minutes used during data collection. To address this issue, we use the voltage disconnect point ($46.2V$) of the discharge as a reference. By aligning the discharge curves at this point, we ensure that they have similar SoC values. Next, we calculate the initial SoC at the start of the discharge by decrementing the SoC backward using the observed load current up to that moment. This method results in a more accurate initial SoC estimate, which is essential to calculate voltage progression using the modified Shepard model.

When complete discharge curves are available, such as in the case of training discharges, they can be aligned to determine the initial SoC. In scenarios where full discharge curves are not available, as in the case of test discharges, the suboptimal initial SoC values obtained by the Coulomb counting method can be used instead. Alternatively, if the operator collects additional data about the battery, more accurate methods can be applied [28]. This work first obtains the initial SoC of all discharges using the alignment method and uses it as input to the battery model.

To quantify the uncertainty of the battery model parameter estimates, a bootstrap method with stratified sampling was used. Stratified sampling was applied for each training discharge curve by dividing the voltage range into three intervals: $v_{\text{batt}} > 48.5$, $48.5 \geq v_{\text{batt}} \geq 47$, and $v_{\text{batt}} < 47$. New discharge curves were generated by sampling an amount of data proportional to the number of samples present in each respective interval. The number of samples in an observed discharge varies depending on the initial SoC values and the magnitude of the discharge load current. An Average Discharge Length (ADL) is calculated from the training discharges by taking the average number of discharge samples. This ADL is then used as a reference for generating stratified samples. To capture the variability in discharge lengths and create a more representative data set, the number of samples generated is varied between 0.75ADL and 1.25ADL. In the experiments, a stratified sampling approach was used to generate 2500 discharge curves. These curves were then used to identify 2500 sets of parameters for the battery model, employing Equation (1) and the least squares approach described in Equation (4). The model parameters obtained are illustrated in the histograms presented in Figure 8. The parameter distributions obtained are skewed. The distribution of A and K takes values typically observed in lead-acid batteries. The distribution of B is skewed towards zero. This parameter represents the sharp exponential decline in the second exponential section of the battery discharge shown in Figure 2. This exponential decline is minimal in both the sampled and real-life discharge data, as can be seen in Figure 8, resulting in B values that are close to zero. The performance of the model parameters obtained is evaluated in subsection IV-C1.

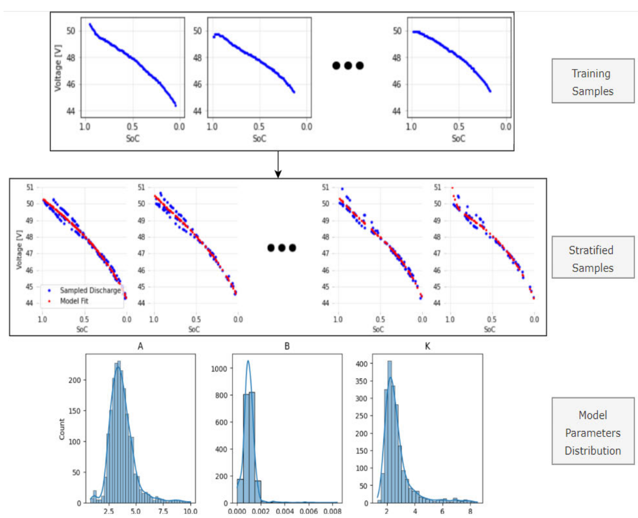

FIGURE 8. Stratified sampling of training data and generation of battery model parameters.

The alternative FNN architecture based battery model comprises two dense layers: the first with 64 neurons and the second with 16 neurons, both employing the Leaky ReLU activation function. The network's final output is a single voltage estimate. Key hyperparameters include the Adam optimizer with a learning rate of 1×10^{-3}, an early stopping criterion with a patience of 10 epochs, a batch size of 16 and a dropout rate of 0.1. The model's training strategy is a "leave-one-out" approach, where one discharge event is set aside for testing while the remaining discharge events are used for training. This strategy enables effective model training and evaluation for battery voltage predictions from the data.

B. LOAD FORECASTING MODEL ARCHITECTURE AND PARAMETER IDENTIFICATION

To predict the voltage progression of a BTS battery using the parameters of the battery model, it is necessary to have the load current values provided by the battery $\hat{i}_{\text{batt}}(t+h)$ over the prediction time horizon $h = 1, \ldots, l$. The future load currents are unknown at the beginning of the discharge process. Therefore, it is necessary to forecast them to predict the voltage progression.

In a BTS power unit, the measured load signifies the total amount of energy required by individual components within the system. A significant portion of the energy demand comes from the mobile network equipment, which is the main customer service provider unit. As can be observed in Figure 9, the load profile exhibits a cyclic pattern with a daily seasonal trend over time, which is closely related to the number of users and devices connected to the system and their activities. Given the load characteristics and the insights presented in Section II-B, a SARIMAX model is adopted to forecast the load currents. During an external power outage, the battery supplies energy to the communication module load and to the control units of the Battery Management System (BMS). This is evident from the increased load current observed after the disconnection, as shown in Figure 9. When an external power source is available, the BMS operates in a low-power idle mode. The proposed model intends to account for the additional energy requirement imposed by the BMS while forecasting through an exogenous variable. The exogenous variable is derived from data about the external power source. It is set a value of 0 when the BTS load is supplied by the external power source. On the other hand, it is set to 1 during power outages and the battery supplies energy to the load.

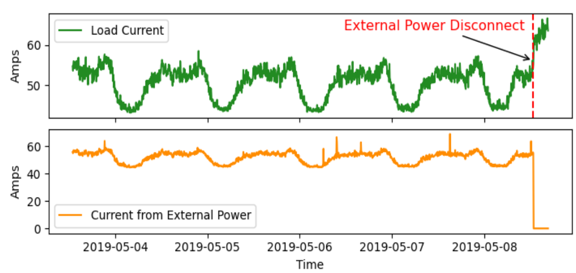

FIGURE 9. BTS load characteristics.

When a discharge event occurs in a BTS, the parameters of the SARIMAX model $(p, d, q)(P, D, Q)$ need to be determined to forecast the expected load current. To train this model, historical load current data observed until the moment of discharge is used. The load characteristics of a BTS during discharge times differ from those during non-discharge times. Thus, the accuracy of the model depends on the amount of historical discharge time load characteristics observed, as it is crucial to capture the load characteristics of future discharge events. For the initial discharges of a BTS, limited previous discharge load characteristic data are available. To address this issue, the load time series data are adjusted by repositioning the initial discharges to a position after the last recorded discharge in the collected data. This method is similar to the leave-one-out approach. For n discharges in a BTS, each discharge will have $n-1$ preceding discharges in the training historical data after the adjustment. Given the daily seasonality of the BTS load characteristics, when a discharge occurrence is relocated to the end, the new position in time is kept on the same day of the week and at a time similar to the original discharge. This adjustment method is illustrated in Figure 10. The initial load section that contains a discharge is swapped with the corresponding later section, ensuring that multiple discharge events are available for model training before making a forecast.

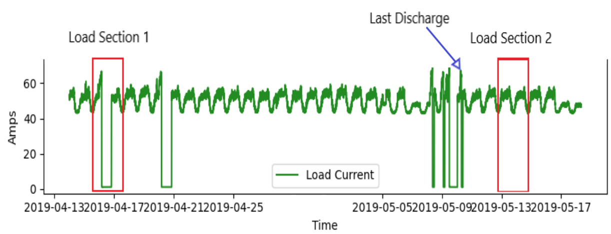

FIGURE 10. Discharge load current repositioning approach to incorporate discharge time load characteristics in training.

Then, the obtained training dataset is used to determine the parameters of the SARIMAX model. This is implemented through a stepwise approach (as provided by the pmdarima library [38]), which searches through multiple combinations of order parameters to select the model that minimizes the Akaike Information Criterion (AIC) score. Figure 11 illustrates three load forecasts generated by this approach, including confidence intervals, from different clusters and BTSs. The forecasts show a low RMSE and closely match the actual load currents.

Based on the best AIC score for the first forecasted discharge in Figure 11, the SARIMAX model of $(5, 0, 2)(1, 0, 1)_{72}$ is obtained and the parameters are provided in Table 3. Given the importance of the daily seasonality trend of the load characteristics in the forecasting, it was found that the differencing orders d and D which provides the minimum AIC value for all discharge load forecasts were zero. For computational efficiency, the original 5-minute sampling time is changed to 20 minutes when building the SARIMAX model. This adjustment results in a daily seasonality of 72 samples (3 samples per hour $\times$ 24).

TABLE 3. Sample SARIMAX model coefficients for a discharge time load forecast.

Term	Coefficient
Autoregressive	$[0.478, -0.071, 0.678, -0.408, -0.366]$
Moving Average	$[-0.637, 0.349]$
Seasonal Autoregressive	$[0.202]$
Seasonal Moving Average	$[0.139]$
Exogenous Variable	$[2.112]$

In Table 4 the performance of the models for each cluster is represented by the RMSE. We can observe from these results that the forecasting models in each cluster have a comparable and consistent performance. The forecasts obtained closely follow the observed load currents, and the confidence interval of the model output gets larger as expected when the forecasting time interval increases, as can be observed from Figure 11. As is typical with forecasting models, the degree of uncertainty tends to grow as the time horizon for the forecast increases.

TABLE 4. RMSE values of forecasted loads per cluster.

Cluster ID	RMSE (in amps)
C1	3.06
C2	2.62
C3	2.62

C. RUT ESTIMATION

In this section, the developed battery model and the load forecasting model are combined to estimate the RUT until the battery voltage threshold reaches 46.2V, which is insufficient to provide full service. Three different scenarios have been designed and experiments corresponding to each scenario were conducted, as illustrated in Figure 12. In these experiments, the RUT is estimated using sampled parameters from the battery model and: 1) actual load measurements, 2) samples from load measurements observed from the historical data around a similar time to the current discharge, and 3) samples from the forecasted load distribution. The first experiment examines the suitability of the developed battery models using true load currents as input. In the second experiment, we assume that the load currents during the current discharge will exhibit characteristics similar to the load currents observed in previously collected data around the same time. Therefore, we sampled these historic load currents to use as input to estimate future discharge voltages. Lastly, we evaluate the proposed integrated approach, which combines the estimated battery model with forecasted load currents using SARIMAX time series forecasting. We then compare and discuss the performance of these three experiments.

Table 5 provides the detailed RUT estimation performance for each discharge using the three experiments. For each

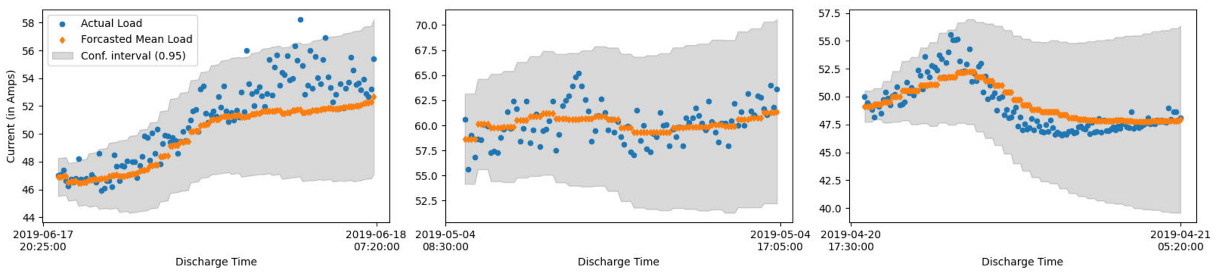

FIGURE 11. SARIMAX-based load forecasting visualization for selected discharges.

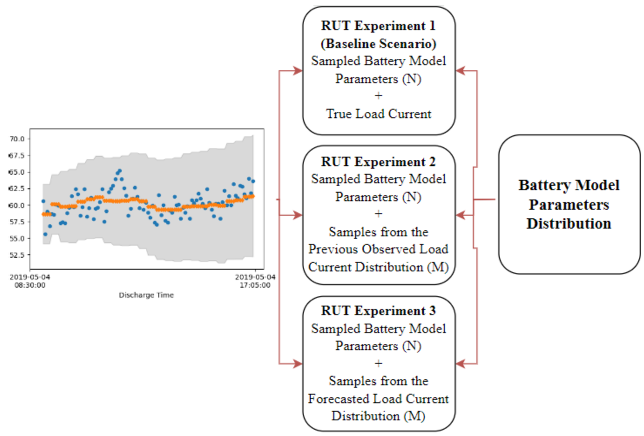

FIGURE 12. RUT experimental setups.

experiment, the RUT_{mean} estimation error is provided along with the corresponding 95% prediction interval to quantify uncertainty. In addition, the MPE results quantify the relative mean error of the RUT estimate with respect to the actual RUT value. Finally, the averages of the absolute mean values of all three metrics are presented.

1) ESTIMATION USING TRUE DISCHARGE LOAD CURRENTS

This section describes a baseline scenario in which the RUT estimate is obtained by using the proposed battery models and the measured load currents as input. It should be noted that this scenario serves merely as a baseline because in reality the load currents will not be known at future time steps beforehand. A PDF plot is used to visualize the distribution of the RUT estimate error for each discharge within a cluster. This plot provides a summary of the essential statistical measures of the 95% prediction interval. The mean of the error distribution is considered the most likely RUT estimation error, while the 2.5% Lower Quantile (LQ) and the 97.5% Upper Quantile (UQ) represent the bounds of the estimation error, representing the uncertainty of the battery model.

Figure 13 illustrates the PDF of errors, defined as the difference between the estimated mean and the actual measured RUT, for four discharges within cluster C1. Using the modified Shepherd battery modeling approach, the errors are generally close to zero. However, the mean is slightly shifted below zero, indicating a tendency to underestimate the RUT. The highest value ME is an underestimation of the RUT by −13.03 minutes for discharge D6, as can be seen in Table 5. Typically, a fully charged battery of this BTS can sustain the load for nearly 4 hours. Therefore, an estimation error of −13.03 minutes or less is relatively minimal. Furthermore, the prediction interval length for this scenario in cluster C1 is at most 15 minutes, indicating limited variability in the RUT estimations.

Overall, the worst performance of this approach, using the relative MPE metric, is an underestimation of −9.72% for discharge D7 in cluster C1, an overestimation of 1.67% for discharge D3 in cluster C2, and an overestimation of −1.52% for discharge D10 in cluster C3. The MPE results are less than 5% of the actual discharge times for 90% of the discharges. The average absolute ME for all discharges is 4.2 minutes with a mean prediction interval of 16.19 minutes.

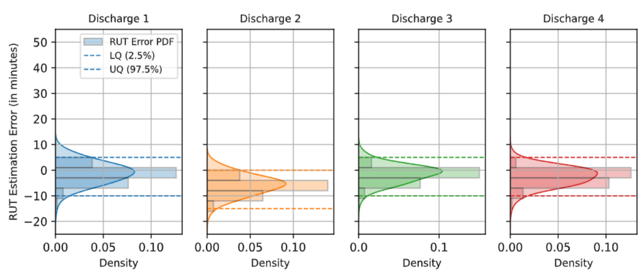

FIGURE 13. PDF of RUT estimation errors in cluster C1 using Modified Shephard battery model. Estimates are based on the measured load current. The bounds represent the 95% prediction interval.

In comparison, Figure 14 shows the PDF of the RUT estimation errors for the four discharges in cluster C1, using the alternative FNN approach discussed in subsection II-A. This battery modeling method tends to significantly overestimate the RUT.

In general, the worst performance of this FNN battery modeling approach, using the relative MPE metric, is an overestimation of 15.88% for discharge D7 in cluster C1, an overestimation of 10.2% for discharge D3 in cluster C2, and an underestimation of 10.77% for discharge D6 in cluster C3. Only 20% of the discharges have an MPE less than 5% of the actual discharge times, which represents a significant decrease compared to the modified Shephard model results. This disparity results from the limited number of discharge

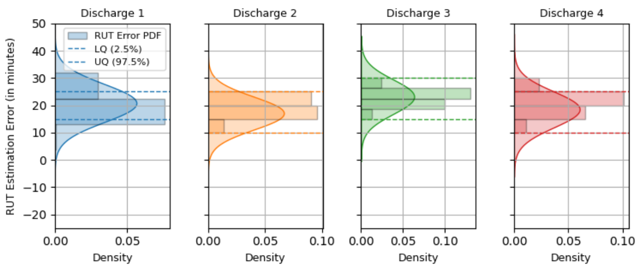

FIGURE 14. PDF of RUT estimation errors in cluster C1 using FNN battery model. Estimates are based on the measured load current.

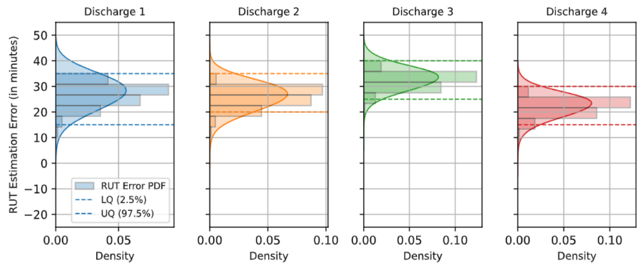

FIGURE 15. PDF of RUT estimation errors in cluster C1. Estimates are based on sampled load currents from previous observed load currents. The bounds represent the 95% prediction interval.

profiles available for training, which has a far greater impact on the FNN approach than on the modified Shepard mathematical modeling approach. Given the superior overall performance of the modified Shepherd model compared to the FNN approach, it has been selected as the preferred battery model for the subsequent experimental results.

2) ESTIMATION USING SAMPLES FROM BOTH BATTERY MODEL PARAMETERS AND PREVIOUS OBSERVED LOAD CURRENTS

In this scenario, the RUT estimation is performed by sampling parameters from both the battery model and the historical load currents of the BTS. To obtain the historical load currents, we consider the start time of the discharge and extract load currents from the preceding days around this time. This approach is based on the observation that the load of a BTS follows a daily cyclic pattern, suggesting that the upcoming discharge will exhibit similar load characteristics to those observed in historical data at the same time of day. This assumption serves as a baseline when actual or forecasted load data are unavailable. Initially, we define an approximate time range for the current discharge. Using this range, we extracted the corresponding load currents from the historical data. These extracted currents are then combined to form a load current set, from which samples will be drawn to estimate the voltage progression of the discharge until the battery voltage drops below the specified threshold.

The results of this approach, as illustrated in Figure 15 for cluster C1, indicate a significant overestimation of the RUT of the batteries. As evident in Table 5, the highest ME for this cluster is an overestimation of 39.67 minutes for discharge D5. The average absolute ME for all discharges is 47.46 minutes, with a mean prediction interval of 18.81 minutes. The worst performance of this approach, based on the MPE metric, includes an overestimation of 26.44% for discharge D5 in cluster C1, 14.18% for discharge D2 in cluster C2, and 18.42% for discharge D7 in cluster C3. The MPE is less than 5% of the actual discharge times for only 9.52% of all discharges, and the average absolute MPE value is 13.47%.

There is a significant increase in the RUT estimation error for this scenario compared to the first scenario. This increase is due to historical sampled load currents, even though the same battery model parameters are used. The load currents were drawn from historical data, but they are not fully representative of the expected load characteristics during the discharge time, even if taken at the same times of the day. As a result, the load current samples taken for the considered discharge may not accurately represent the expected load characteristics. These samples often have much smaller values compared to the actual discharge-time load currents, leading to a substantial overestimation of the RUT values.

3) ESTIMATION USING SAMPLES FROM BOTH BATTERY MODEL PARAMETERS AND FORECASTED DISCHARGE LOAD CURRENTS

In this scenario, the RUT estimation is performed by sampling from the distributions of the parameters of the battery model and forecasted load currents. Two models, the battery model and the load forecasting model, are devised to produce the RUT estimates. Consequently, the uncertainty in the estimation arises from both the battery model and the load forecasting model. This is evident from the larger overall mean prediction interval of 26.43 minutes shown in Table 5, which is higher than the uncertainty observed in the initial two scenarios.

Regarding the mean RUT estimation error, we expect this scenario to perform less effectively compared to scenario 1, which uses the true load current. This is observed in the overall ME and relative MPE metrics. In this scenario, the values of ME and MPE are 12.61 minutes and 3.15%, respectively, which are higher than the values obtained in scenario 1, which are 4.20 minutes and 1.78%. However, when examining individual discharges, the RUT estimates in this scenario may not always perform worse than in Scenario 1. Focusing on cluster 1, discharges D2, D6, and D7 demonstrate this behavior, as presented in Table 5. This occurs because the battery model might underestimate the RUT when predicting with the true load currents. However, if the forecasted load for a discharge is lower than the actual load currents, this can lead to an overestimation of the RUT. When RUT estimations are made using an underestimating battery model in combination with lower-than-actual load forecasts, the accuracy of the estimations improves. This behavior is observed in multiple discharges from all clusters.

TABLE 5. RUT estimation error of all discharges.

		ME (in minutes)			Prediction Interval [LQ, UQ] (in minutes)			MPE (in %)		
Cluster ID	Discharge ID	Scenario 1	Scenario 2	Scenario 3	Scenario 1	Scenario 2	Scenario 3	Scenario 1	Scenario 2	Scenario 3
C1	D1	−1.37	27.57	2.78	[−10, 5]	[15, 35]	[−5, 10]	−1.05	21.21	2.14
	D2	−6.02	26.05	−0.15	[−15, 0]	[20, 30]	[−10, 10]	−4.30	18.61	−0.11
	D3	−1.69	33.05	4.29	[−10, 5]	[25, 40]	[−5, 15]	−1.09	21.32	2.77
	D4	−2.80	22.55	5.23	[−10, 5]	[15, 30]	[−5, 20]	−1.60	12.89	2.99
	D5	1.30	39.67	12.06	[−5, 5]	[30, 45]	[5, 20]	0.87	26.44	8.04
	D6	−13.03	5.16	−9.43	[−20, −5]	[−5, 10]	[−20, 0]	−8.69	3.44	−6.29
	D7	−6.32	8.72	−5.12	[−15, 0]	[0, 20]	[−15, 5]	−9.72	13.41	−7.88
C2	D1	8.09	52.61	−13.78	[0, 10]	[40, 60]	[−25, −5]	1.40	9.07	−2.38
	D2	−2.39	73.74	12.33	[−10, 0]	[65, 80]	[5, 20]	−0.46	14.18	2.37
	D3	10.67	69.98	39.22	[0, 15]	[60, 75]	[25, 50]	1.67	10.93	6.13
	D4	3.73	75.40	−9.07	[−5, 10]	[65, 80]	[−20, 0]	0.54	10.93	−1.31
C3	D1	1.62	67.55	16.13	[−10, 10]	[55, 75]	[5, 30]	0.34	14.07	3.36
	D2	−6.22	61.93	−4.70	[−15, 0]	[55, 70]	[−15, 10]	−1.23	12.26	−0.93
	D3	1.15	71.24	22.12	[−10, 10]	[60, 85]	[5, 40]	0.21	13.07	4.06
	D4	0.28	36.57	23.26	[−10, 10]	[25, 50]	[5, 45]	0.06	7.62	4.85
	D5	3.67	57.85	21.98	[−5, 10]	[50, 65]	[0, 45]	0.74	11.69	4.44
	D6	−1.47	31.05	0.76	[−10, 5]	[20, 40]	[−10, 15]	−0.75	15.92	0.39
	D7	0.56	86.59	21.77	[−10, 10]	[75, 100]	[0, 55]	0.12	18.42	4.63
	D8	−0.57	52.63	23.04	[−10, 10]	[40, 60]	[5, 45]	−0.13	11.96	5.24
	D9	−5.73	71.63	9.28	[−15, 5]	[55, 85]	[−5, 25]	−0.90	11.28	1.46
	D10	−9.48	25.20	−8.42	[−20, 5]	[15, 40]	[−20, 0]	−1.52	4.03	−1.35
	Average of absolutes	**4.20**	**47.46**	**12.61**	**16.19**	**18.81**	**26.43**	**1.78**	**13.47**	**3.48**

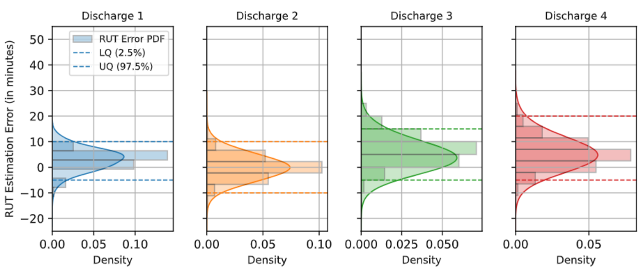

FIGURE 16. PDF of RUT estimation errors in cluster C1. Estimates are based on samples from the distribution of the forecasted load current. The bounds represent the 95% prediction interval.

If this scenario achieves better RUT estimations compared to scenario 2, we can infer that the forecasting method devised here provides a more accurate prediction of future discharge load currents. This method performs better than the straightforward approach of assuming that future load currents will resemble the previous load currents in the historical load data and using samples from it. Figure 16 presents the improved results of RUT estimation using this approach, highlighting the improvements compared to Figure 15, for some discharges in cluster C1. The averaged absolute ME and relative MPE metrics for this scenario are 12.61 minutes and 3.15%, respectively, which are significantly lower than the metrics obtained in Scenario 2, which were 47.46 minutes and 13.47%. This indicates that the estimation error with the new approach is roughly a quarter of that of Scenario 2.

V. CONCLUSION

A battery in a BTS system is a critical component, and it keeps the system afloat in a standalone manner or in conjunction with other external power sources. This work addresses the issue of estimating the energy depletion time under different load conditions. This is achieved using a battery model and also by forecasting future loads during a discharge state.

The baseline scenario, devised to validate the battery model using modified Shepherd equations, demonstrated good RUT performance with an average absolute MPE of 1.78% compared to the actual observed values. This corresponds to a relative error of less than 2%. Considering that the primary data available about batteries are their discharge curves and limited specifications, the proposed battery modeling approach is well-suited for the use case scenario. In reality, the load currents are not known in advance and must be estimated. A simple and straightforward method relies on the assumption that future discharge loads will be similar to the load currents observed previously at the same time as the current discharge. Samples were then taken from these previous observations. These samples are then used to determine the voltage progression of the battery during discharge. When estimating the RUT using this approach, the average absolute MPE increased to 13.47%, which is more than seven times the baseline scenario. Thus, to improve the RUT estimation, we developed a load forecasting model in addition to the battery model. Using the SARIMAX model to forecast the discharge load current, chosen based on the initial analysis of the BTS load characteristics, we observed improved performance. The average absolute MPE was reduced to 3.48%. However, one drawback is the increased uncertainty in RUT estimation because the approach now requires two models. This uncertainty was quantified using a prediction interval, showing an increase from 16.19 in the baseline case to 18.81 in the second scenario, and ultimately to 26.43 minutes for the proposed approach. Overall, the estimates are considered satisfactory given that the batteries can sustain the load for hours.

For the telecom operator examined in this study, the implementation of an automated framework to address BTS power interruptions has the potential to substantially improve the development of effective intervention strategies. The findings of this research serve as a valuable supplementary tool for the operator's engineering team, particularly for those who currently rely heavily on their experience when making critical decisions. A notable limitation of this work is the limited dataset provided by the operator, which precluded the application of state-of-the-art deep learning methodologies. However, with continued data collection in the future, it will be possible to construct more robust models, further enhancing the accuracy and reliability of the RUT estimation process.

REFERENCES

[1] T. Heskes, "Practical confidence and prediction intervals," in *Proc. Adv. Neural Inf. Process. Syst.*, 1997, pp. 176–182.

[2] L. Liao and F. Köttig, "Review of hybrid prognostics approaches for remaining useful life prediction of engineered systems, and an application to battery life prediction," *IEEE Trans. Rel.*, vol. 63, no. 1, pp. 191–207, Mar. 2014.

[3] L. Ren, L. Zhao, S. Hong, S. Zhao, H. Wang, and L. Zhang, "Remaining useful life prediction for lithium-ion battery: A deep learning approach," *IEEE Access*, vol. 6, pp. 50587–50598, 2018.

[4] J. N. C. Sekhar, B. Domathoti, and E. D. R. S. Gonzalez, "Prediction of battery remaining useful life using machine learning algorithms," *Sustainability*, vol. 15, no. 21, p. 15283, Oct. 2023.

[5] D. Doerffel and S. A. Sharkh, "A critical review of using the Peukert equation for determining the remaining capacity of lead-acid and lithium-ion batteries," *J. Power Sources*, vol. 155, no. 2, pp. 395–400, Apr. 2006.

[6] L. A. Vicari, V. A. De Lima, A. S. De Moraes, and M. C. Lopes, "Remaining capacity estimation of lead-acid batteries using exponential decay equations," *Orbital, Electron. J. Chem.*, vol. 13, no. 5, pp. 392–398, Dec. 2021.

[7] P. Rong and M. Pedram, "An analytical model for predicting the remaining battery capacity of lithium-ion batteries," *IEEE Trans. Very Large Scale Integr. (VLSI) Syst.*, vol. 14, no. 5, pp. 441–451, May 2006.

[8] N. Daniil, D. Drury, and P. H. Mellor, "Performance comparison of diffusion, circuit-based and kinetic battery models," in *Proc. IEEE Energy Convers. Congr. Expo. (ECCE)*, Sep. 2015, pp. 1382–1389.

[9] V. S. Deshpande and R. M. Mcmeeking, "Models for the interplay of mechanics, electrochemistry, thermodynamics, and kinetics in lithium-ion batteries," *Appl. Mech. Rev.*, vol. 75, no. 1, Jan. 2023, Art. no. 010801.

[10] W. H. Cui, J. S. Wang, and Y. Y. Chen, "Equivalent circuit model of lead-acid battery in energy storage power station and its state-of-charge estimation based on extended Kalman filtering method," *Eng. Lett.*, vol. 26, no. 4, pp. 504–517, 2018.

[11] B. S. Bhangu, P. Bentley, D. A. Stone, and C. M. Bingham, "Nonlinear observers for predicting state-of-charge and state-of-health of lead-acid batteries for hybrid-electric vehicles," *IEEE Trans. Veh. Technol.*, vol. 54, no. 3, pp. 783–794, May 2005.

[12] X. Zheng and H. Fang, "An integrated unscented Kalman filter and relevance vector regression approach for lithium-ion battery remaining useful life and short-term capacity prediction," *Rel. Eng. Syst. Saf.*, vol. 144, pp. 74–82, Dec. 2015.

[13] S. Zhao, C. Zhang, and Y. Wang, "Lithium-ion battery capacity and remaining useful life prediction using board learning system and long short-term memory neural network," *J. Energy Storage*, vol. 52, Aug. 2022, Art. no. 104901.

[14] S. Wang, S. Jin, D. Bai, Y. Fan, H. Shi, and C. Fernandez, "A critical review of improved deep learning methods for the remaining useful life prediction of lithium-ion batteries," *Energy Rep.*, vol. 7, pp. 5562–5574, Nov. 2021.

[15] D. R. S. Nugraha, A. B. Pangestu, and F. Husnayain, "State of charge estimation of lead-acid battery with Coulomb counting and feed-forward neural network method," in *Proc. FORTEI-Int. Conf. Electr. Eng. (FORTEI-ICEE)*, Sep. 2020, pp. 119–124.

[16] Y. Su, H. Zhou, N. Zhou, C. Li, X. Wang, and D. Wang, "Soft computing detection method for remaining capacity of lead-acid battery," in *Proc. IEEE 4th Int. Conf. Comput. Commun. (ICCC)*, Dec. 2018, pp. 2631–2634.

[17] K. Kutluay, Y. Cadirci, Y. S. Ozkazanc, and I. Cadirci, "A new online state-of-charge estimation and monitoring system for sealed lead–acid batteries in telecommunication power supplies," *IEEE Trans. Ind. Electron.*, vol. 52, no. 5, pp. 1315–1327, Oct. 2005.

[18] H. Ertan, A. Yavariabdi, S. E. Küçükbay, A. Emre Tiryaki, E. Aksoy, and I. B. Özalp, "Lead-acid battery lifetime estimation using limited labeled data for cellular base stations," in *Proc. Wireless Telecommun. Symp. (WTS)*, Apr. 2022, pp. 1–7.

[19] P. E. Pascoe and A. H. Anbuky, "VRLA battery discharge reserve time estimation," *IEEE Trans. Power Electron.*, vol. 19, no. 6, pp. 1515–1522, Nov. 2004.

[20] G. L. Plett, *Battery Management Systems, Volume II:, Equivalent-circuit Methods*. Norwood, MA, USA: Artech House, 2015.

[21] D. N. T. How, M. A. Hannan, M. S. H. Lipu, and P. J. Ker, "State of charge estimation for lithium-ion batteries using model-based and data-driven methods: A review," *IEEE Access*, vol. 7, pp. 136116–136136, 2019.

[22] W. Zhou, Y. Zheng, Z. Pan, and Q. Lu, "Review on the battery model and SOC estimation method," *Processes*, vol. 9, no. 9, p. 1685, Sep. 2021.

[23] H. He, R. Xiong, H. Guo, and S. Li, "Comparison study on the battery models used for the energy management of batteries in electric vehicles," *Energy Convers. Manage.*, vol. 64, pp. 113–121, Dec. 2012.

[24] S. Li and B. Ke, "Study of battery modeling using mathematical and circuit oriented approaches," in *Proc. IEEE Power Energy Soc. Gen. Meeting*, Jul. 2011, pp. 1–8.

[25] S. Tamilselvi, S. Gunasundari, N. Karuppiah, R. K. A. Razak, S. Madhusudan, V. M. Nagarajan, T. Sathish, M. Z. M. Shamim, C. A. Saleel, and A. Afzal, "A review on battery modelling techniques," *Sustainability*, vol. 13, no. 18, p. 10042, Sep. 2021.

[26] C. M. Shepherd, "Design of primary and secondary cells," *J. Electrochem. Soc.*, vol. 112, no. 7, p. 657, 1965.

[27] O. Tremblay, L.-A. Dessaint, and A.-I. Dekkiche, "A generic battery model for the dynamic simulation of hybrid electric vehicles," in *Proc. IEEE Vehicle Power Propuls. Conf.*, Sep. 2007, pp. 284–289.

[28] S. Piller, M. Perrin, and A. Jossen, "Methods for state-of-charge determination and their applications," *J. Power Sources*, vol. 96, no. 1, pp. 113–120, Jun. 2001.

[29] E. Chemali, P. J. Kollmeyer, M. Preindl, and A. Emadi, "State-of-charge estimation of Li-ion batteries using deep neural networks: A machine learning approach," *J. Power Sources*, vol. 400, pp. 242–255, Oct. 2018.

[30] M. Charkhgard and M. Farrokhi, "State-of-charge estimation for lithium-ion batteries using neural networks and EKF," *IEEE Trans. Ind. Electron.*, vol. 57, no. 12, pp. 4178–4187, Dec. 2010.

[31] C. Z. Mooney, R. D. Duval, and R. Duvall, *Bootstrapping: A Nonparametric Approach To Statistical Inference*. Newbury Park, CA, USA: Sage, 1993.

[32] C. Kuster, Y. Rezgui, and M. Mourshed, "Electrical load forecasting models: A critical systematic review," *Sustain. Cities Soc.*, vol. 35, pp. 257–270, Nov. 2017.

[33] F. M. Bianchi, E. Maiorino, M. C. Kampffmeyer, A. Rizzi, and R. Jenssen, "An overview and comparative analysis of recurrent neural networks for short term load forecasting," 2017, *arXiv:1705.0437*.

[34] S. Siami-Namini, N. Tavakoli, and A. S. Namin, "A comparison of ARIMA and LSTM in forecasting time series," in *Proc. 17th IEEE Int. Conf. Mach. Learn. Appl. (ICMLA)*, Dec. 2018, pp. 1394–1401.

[35] S. I. Vagropoulos, G. I. Chouliaras, E. G. Kardakos, C. K. Simoglou, and A. G. Bakirtzis, "Comparison of SARIMAX, SARIMA, modified SARIMA and ANN-based models for short-term PV generation forecasting," in *Proc. IEEE Int. Energy Conf. (ENERGYCON)*, Apr. 2016, pp. 1–6.
[36] *ZXDU68 T601 DC Power System*, ZTE Corp., Shenzhen, China, 2008.
[37] T.-T. Wong, "Performance evaluation of classification algorithms by k-fold and leave-one-out cross validation," *Pattern Recognit.*, vol. 48, no. 9, pp. 2839–2846, Sep. 2015.
[38] T. G. Smith et al. (2017). *pmdarima: ARIMA Estimators for Python*. Accessed: May 9, 2024. [Online]. Available: http://www.alkaline-ml.com/pmdarima and https://alkaline-ml.com/pmdarima/develop/citing.html

YONAS TEFERA (Member, IEEE) received the B.S. degree in electrical engineering from Haramaya University, Haramaya, Ethiopia, in 2009, and the M.S. degree in computer and communication networks engineering from the Politecnico di Torino, Turin, Italy, in 2013. He is currently pursuing the Ph.D. degree with the Faculty of Engineering Technology, KU Leuven, Geel, Belgium. His research interests include anomaly detection, fault diagnostics, and predictive maintenance of engineering assets through the use of machine learning algorithms.

STIJN LUCA received the M.Sc. degree in mathematics from KU Leuven, Belgium, in 2003, and the Ph.D. degree in mathematics from Hasselt University, Belgium, in 2007.

He is currently an Associate Professor with the Department of Data Analysis and Mathematical Modelling, Faculty of Bioscience Engineering, Ghent University, Belgium. Previously, he was a Postdoctoral Fellow with KU Leuven and a Visiting Scholar with the University of Oxford, from 2014 to 2015. His research interests include the theory and methods of statistical data analysis and their applications.

DEREJE HAILEMARIAM WOLDEGEBREAL received the Ph.D. degree in electrical engineering from the University of Paderborn, Germany, in 2010, with a focus on network coding for wireless cooperative communication. Since 2011, he has been an Associate Professor with the School of Electrical and Computer Engineering, Addis Ababa University (AAU). His current research interests include the intersection of machine learning and telecommunications systems, with a focus on network and service quality evaluation, spectrum utilization optimization, mobile data traffic prediction, and energy management in telecom networks. He also explores the application of information theory to Ethiopian languages. In addition to his academic contributions through numerous publications in journals and conferences, he has assumed various administrative responsibilities within AAU, engages with professional associations, and is dedicated to applying AI tools for process automation and optimizing business operations in the private sector.

PETER KARSMAKERS received the M.Sc. degree in artificial intelligence and the Ph.D. degree from the Department of Electrical Engineering, KU Leuven, in 2004 and 2010, respectively. From 2010 to 2013, he was a Postdoctoral Researcher with the Mobilab Research Group, Thomas More. From 2013 to 2018, he was a Postdoctoral Researcher with KU Leuven, where he cofounded the Advanced Integrated Sensing (ADVISE) Research Team. Currently, he is an Associate Professor with the Computer Science Department, Declarative Languages and Artificial Intelligence (DTAI) Section, KU Leuven, and is a member of the Leuven.AI Institute. Since 2022, he has been a Principal Investigator of Flanders Make@KU Leuven. His research interests include designing machine learning algorithms that consider application-specific constraints like the computing platform, need for physical consistency, and limited availability of annotated data. He worked on diverse industrial collaboration projects that involve monitoring applications using microphones, accelerometers, and radars.